Microwave-Assisted Chemical Co-reduction of Pd Nanoparticles Anchored on Reduced Graphene Oxide with Different Loading Amounts

Dyah Ayu Fatmawati, Triyono Triyono*, Wega Trisunaryanti, and Uswatul Chasanah

Department of Chemistry, Faculty of Mathematics and Natural Sciences, Universitas Gadjah Mada, Sekip Utara, Yogyakarta 55281, Indonesia

** Corresponding author:*

email: triyn102@ugm.ac.id

Received: February 22, 2022
Accepted: August 10, 2022

DOI: 10.22146/ijc.73206

Abstract: *Microwave-assisted Palladium/Reduced Graphene Oxide (Pd/RGO) synthesis was effectively carried out in this study, which looked at the effects of different Pd loading weights in Graphene Oxide (GO) on its physicochemical qualities. The Tour technique was used to make GO, with a $KMnO_4$:graphite weight ratio of 3.5. Meanwhile, Pd/RGO was synthesized utilizing the in-situ reduction method of one-pot synthesis with ascorbic acid as the green reducing agent, yielding Pd-0.5/RGO, Pd-1.0/RGO, and Pd-2.0/RGO, respectively, with variations in Pd loading weight of 0.5, 1.0, and 2.0%. XRD, FTIR, SAA, SEM-EDX, and TEM were used to examine all material characterizations. As a result, Pd-1.0/RGO had the largest surface area of 65.168 m^2/g among the Pd-based materials, with a pore volume of 0.111 cc/g, the pore diameter of 3.316 nm, Pd crystallite size of 28.29 nm, RGO nanostructure dimension of 3.37 × 28.53 nm, and reduction level (C/O) of 3.02. This material also contains specific functional groups, including O-H, C-H, CO_2, C=C, C=O, and C-O, based on FTIR spectra. Therefore, optimal weight loading of metal on the surface of the supporting material will provide a large material surface area. Increasing the surface area of the material improves its performance as a catalyst.*

Keywords: *in-situ reduction; palladium; reduced graphene oxide; microwave, Tour method*

■ INTRODUCTION

For graphene-based applications in electronics, optics, chemistry, energy storage, and biology, graphene oxide (GO) is a valuable and promising material [1]. Graphene oxide is graphite oxidized to allow oxygen molecules to intersperse between the carbon layers [2]. Although the actual structure of GO is unknown, it is evident that epoxides, alcohols, ketone carbonyls, and carboxylic groups disrupt the previously contiguous aromatic lattice of graphene [3]. Various advantages over graphene, such as more excellent solubility [4] and the ability to surface functionalize, are due to these oxygenated groups, which have opened up many possibilities for application in nanocomposite materials [5]. For GO synthesis, chemical approaches based on oxidative-exfoliation processes have been developed over time [6]. The most popular technique was developed by Hummers and employed potassium permanganate ($KMnO_4$) and sodium nitrate ($NaNO_3$). [7]. The Hummers method was additionally enhanced by omitting $NaNO_3$ to prevent the production of harmful gases, using ice in place of liquid water to prevent a high-temperature rise and thereby promoting better and easier control of the reaction, increasing yield and oxidation degree while promoting the retention of carbon rings in the basal plane by adding phosphoric acid (H_3PO^4) to the reaction medium and omitting $NaNO_3$ altogether. This approach is called Tour approach [8].

The oxidative-exfoliation procedures can yield vast amounts of GO, but a graphene-like nanosheet requires further treatment to reduce it into reduced graphene oxide (RGO) [9]. Ascorbic acid (L-AA) is an affordable and plentiful material that can reduce GO to an acceptable level as a green alternative to standard reducing agents of GO (e.g., hydrazine hydrate and

sodium borohydride) [10]. More importantly, compared to the traditional reductants employed in GO reduction, L-AA and its oxidized products are environmentally beneficial [11]. Despite the widespread use of strong reducing chemicals to reduce GO, the process is still exceedingly slow. Microwave irradiation was discovered to speed up the reduction rate [12] significantly. Microwaves heat materials directly through dielectric loss rather than heat convection, as in traditional heating methods, allowing for rapid and precise heating [13]. It is thought to be promising in reducing reaction time and producing hot spots with extremely high temperatures.

Palladium (Pd) is a platinum (Pt) group metal with numerous uses in medicine, the environment, and materials research. Pd is a unique metal with a wide range of catalytic applications in various industries at ambient temperatures [14]. Compared to Pt-based catalysts, Pd is a more effective catalyst for the Formate Oxidation Reaction (FOR) in both half-cell and fuel cell tests [15]. Because of their high surface-to-volume ratio and more active/selective surface atoms than bulk Pd catalysts, Pd nanoparticles (PdNPs) have gained much attention in organic synthesis in recent years [16]. PdNPs are a hot topic because of their high catalytic activity and the possibility of being employed as heterogeneous catalysts with unique features. As a support material of PdNPs, RGO is more commonly utilized than other carbon-based materials such as porous carbon and carbon nanotubes because of its high availability, excellent corrosion resistance, low cost, and superior dispersion in nature [17].

There are many reports regarding the synthesis of Pd/RGO compounds. Wang et al. researched the usage of reducing agents such as ethylene glycol, sodium borohydride, and hydrazine hydrate in a comparative study [18]. Kumar et al. synthesized Pd/RGO by microwave-assisted heating reduction but using GO precursor produced from the modified Staudenmaier method [19]. Ng et al. investigated the Pd/RGO using GO precursor synthesized by Tour technique, but through ultrasonic wave-assisted reduction heating type [20]. Furthermore, Li et al. made Pd/RGO under microwave irradiation but used ethylene glycol as a reducing agent [21]. Therefore, in this work, we investigated the Pd/RGO utilizing the GO precursor obtained from the Tour method. This GO preparation was adapted from Fatmawati et al., which used a weight of oxidizing agent for graphite of 3.5 [22], which is lower than the usual value of 6. Then the Pd/RGO synthesis was carried out by microwave-assisted in-situ reduction heating using ascorbic acid. Consequently, the goal of this study is to improve on earlier research by employing a shorter and simpler reduction heating, using GO precursor with a lower ratio of oxidizing agent to graphite than recommended by the Tour method, as well as utilizing ascorbic acid as a green reducing agent. The characterization data of the XRD, FTIR, SAA, SEM-EDX, and TEM will be used to investigate further the physicochemical properties of the Pd/RGO material.

■ EXPERIMENTAL SECTION

Materials

All the ingredients used in this experiment came from commercial sources (E-Merck Germany, p.a.) and were used without being purified. Graphite powder, Potassium permanganate ($KMnO_4$, H_2SO_4 98%), Orthophosphoric acid (H_3PO_4 85%), Hydrogen peroxide (H_2O_2 30%), Hydrochloric acid (HCl 37%), absolute ethanol, L(+)-Ascorbic acid, Palladium(II) chloride ($PdCl_2$) anhydrous, Sodium hydroxide (NaOH), Silver nitrate ($AgNO_3$), Barium chloride dihydrate ($BaCl_2{\cdot}2H_2O$), deionized (DI) water, phosphate-buffered saline (PBS), and bidistilled water were among the materials utilized.

Instrumentation

The crystallinity of the materials was determined by X-Ray Diffraction (Bruker D2 Phaser) at a wide angle of 5–90°. The materials' functional groups were determined using a Fourier Transform Infrared Spectrometer (FTIR, Shimadzu Prestige 21) operating at 4000–400 cm^{-1}. The Surface Area Analyzer (SAA, JWGB Meso 112) was used to examine the textural features of materials, including specific surface area, pore volume, and pore diameter, which were determined using the BET and BJH methods. Using a Transmission Electron Microscope, the materials' structure and polycrystalline

ring pictures were captured (TEM, JEOL JEM-1400). Scanning Electron Microscope-Energy Dispersive X-ray spectroscopy was used to examine the materials' surface morphology and metal content (SEM-EDX, JSM-6510LA).

Procedure

Synthesis of graphene oxide (GO)

$KMnO_4$ 1.3125 g was mixed with 0.375 g graphite powder (weight ratio of 3.5) and placed in Beaker I [22]. Then, in Beaker II, 45 mL H_2SO_4 and 5 mL H_3PO_4 (volume ratio of 9) were added. For 1 h, the two beakers were placed in a cooler box with ice. Then, while stirring, the solution in Beaker II was transferred to Beaker I and heated for six hours at 65 °C [23]. The solution was then placed into another beaker containing 200 g DI water ice and 3 mL H_2O_2 and swirled with a stirring rod. The solids GO were left to precipitate in the solution. GO was washed with a solution of HCl (2 times), ethanol absolute (2 times), and PBS at 5000 rpm for 5 min until the pH of the solution reached 7. The solution was then tested for chloride ions using $AgNO_3$ and sulfate ions using $BaCl_2$. The washing process was repeated numerous times using hot bi-distilled water until the solution was free of both. Finally, the solid was dried for 12 h at 80 °C in an oven.

Synthesis of palladium/reduced graphene oxide (Pd/RGO)

The in-situ approach was used to deposit metal nanoparticles onto the RGO surface. First, each $PdCl_2$ salt precursor solution (with 0.5, 1.0, and 2.0 percent w/w Pd metal loading on GO) was agitated for 10 min at room temperature before being added to the GO dispersion (0.3 g in 25 mL distilled water). After stirring for 10 min, the pH of the reaction mixture was raised to 9 by adding 0.1 M NaOH solution. After 5 min of stirring, a 3 g ascorbic acid reducing agent was added to the reaction mixture (weight ratio of ascorbic acid to GO of 10). Stirring was continued for 10 min, followed by microwave-assisted heating for 4 min at 70 °C with high frequency using a microwave instrument (Electrolux, Model EMM2308X). The Pd/RGO nanostructures were rinsed numerous times with distilled water until they reached a neutral pH and then dried for 12 h at 60 °C. An illustration of the Pd/RGO synthesis procedure is briefly shown in Fig. 1.

■ RESULTS AND DISCUSSION

Analysis of Material Crystallinity

XRD measurements were used to determine the crystalline phase structure of the samples. The diffractograms of GO and Pd/RGO with various metal loading levels are shown in Fig. 2. GO material is made from graphite, which has a typical peak at about 26° and a characteristic spacing between graphene layers of 0.34 nm, according to Fatmawati et al. [24]. The expanded layer spacing after the graphite oxidation process was caused by the oxygen functional groups from oxidants

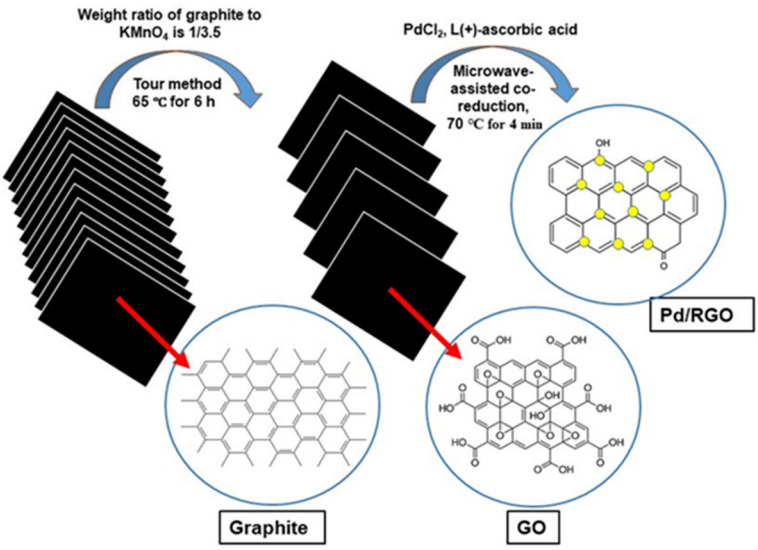

Fig 1. The illustration of the Pd/RGO synthesis procedure

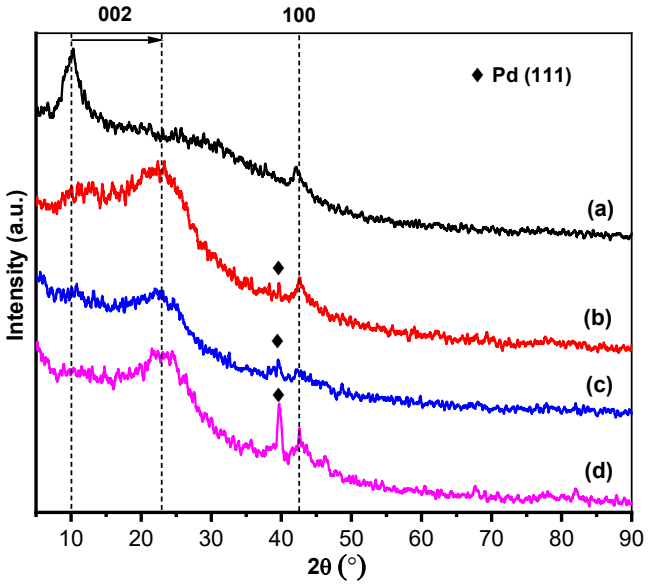

Fig 2. Diffractogram of (a) GO (b) Pd-0.5/RGO (c) Pd-1.0/RGO (d) Pd-2.0/RGO

attached on both sides of the graphene sheets, as well as the resulting atomic-scale roughness to the originally atomically flat graphene sheets [25]. During the oxidation process, the d-spacing increases from 0.34 to 0.87 nm, resulting in around a 150% increase in distance between layers in GO compared to pristine graphite. The result of this study is slightly lower than that of Bera et al. [26]. This effect is owing to changes in oxidation treatment, with ultrasonic waves being used in some cases. The d value for GO, according to Prabakaran et al., is between 0.6 and 1 nm [27]. The peak of GO at 10.19° vanishes after reduction treatment, and a new peak forms at 22–23°, which belongs to RGO's C(002) planes, showing that GO sheets were successfully reduced by microwave irradiation for all samples [28]. Furthermore, each line of Pd/RGO has a large peak at 22–23°, which is attributed to the (002) planes of RGO, implying the removal of oxygen-containing functional groups from the GO [29]. The shift from a sharp to a broad peak form implies that removing oxygen groups from the graphene sheet produces crystal damage or flaws. The gap between the graphene layers was reduced from 0.87 to 0.40 nm when these groups were removed. Furthermore, the peaks near 40° could be attributed to the (111) lattice planes of Pd's face-centered cubic crystalline structure (JCPDS No. 46-1043) [20]. Due to the minimal quantity of metal loading on the support material, the crystal plane of Pd (200), (220), and (311) is missing. The diffractogram shows that increasing the amount of metal loading on the support material enhances the intensity of crystallinity while decreasing the crystallite size (CS), as reported by Ng et al. [20]. The Scherrer equation is used to obtain these values, which are based on the Scherrer constant (K = 0.9) and the height (H) of the carbon nanostructure. Following Stobinski et al., the diameter (D) of the carbon nanostructure was determined using the Warren constant (K = 1.84) [30]. As a result, the stacked carbon nanostructure has dimensions of D x H with a layer separation of d. The findings of the XRD spectra interpretation calculation are shown in Table 1.

Analysis of Material Typical Functional Groups

The rise and decrease in the spacing between layers (d) of graphite–GO–Pd/RGO are connected to the presence of oxygen functional groups, as shown in earlier XRD data in Table 1. Fig. 3 shows FTIR spectra that confirmed this type of oxygen functional group. Firm peaks in the GO spectra can be found at 3400 and 1600–1700 cm^{-1}. OH vibrations from alcohol and carboxylic acid groups, as well as water absorption, are related to these peaks, as are C=O vibrations from ketone, carboxylic acid, and ester groups. C-H vibrations from sp^3 conjugated

Table 1. Data interpretation of XRD analysis

Material	Peak characteristic of carbon material					Peak of Pd	
	2θ (002)	d (nm)	H (nm)	2θ (100)	D (nm)	2θ (111)	CS (nm)
GO	10.19	0.87	2.71	42.08	15.93	-	-
Pd-0.5/RGO	22.01	0.40	1.71	42.64	17.59	39.68	23.77
Pd-1.0/RGO	22.00	0.40	3.37	42.30	28.53	39.59	28.29
Pd-2.0/RGO	23.03	0.39	2.10	42.60	5.79	39.74	14.42

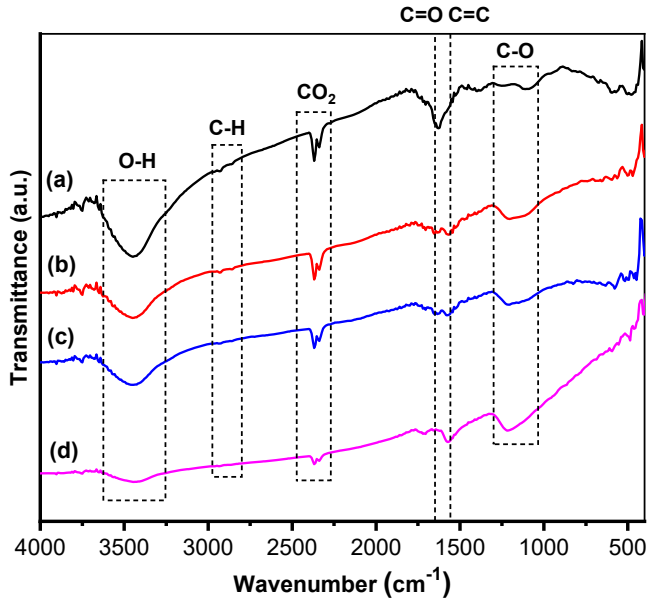

Fig 3. FTIR spectra of (a) GO (b) Pd-0.5/RGO (c) Pd-1.0/RGO (d) Pd-2.0/RGO

carbons, C=C vibrations from graphitic carbons, and C-O vibrations from alcohol, alkoxy, carboxylic, and ester groups are represented by lesser intensity peaks at 2800–2900, 1500–1600, and 1000–1300 cm^{-1} [31]. The peak at 3400 cm^{-1} reduced in strength, and the peak at 1600–1700 cm^{-1} diminished after reduction using a combination of microwave-assisted heating and a reducing agent in the form of ascorbic acid, showing carboxylic group breakdown [30]. The remaining oxygen-containing functional groups after the reduction process, according to the spectra, are hydroxyl and epoxy. Meanwhile, because metal deposition on RGO did not produce any absorption band linked with Pd-O, the effect of metal loading cannot be substantiated using these results [32]. As a result, the three materials have pretty similar personalities. Table 2 shows the complete results of the FTIR interpretation.

Analysis of Material Elemental Composition

Furthermore, the percentage of elements present in the material, particularly oxygen functional groups, can be estimated using EDX calculations based on earlier FTIR data. The EDX data shows the investigation results with percent mass C increasing and percent mass O decreasing from GO to Pd/RGO. This finding shows that the process of reduction was successful.

The FTIR results follow the hypothesis that RGO materials primarily comprise carbon. The C/O ratio represents the reduction level, with a more excellent ratio indicating that more oxygen groups in the substance have been reduced. Due to leaching during material washing, the actual percent mass of Pd was lower than that deposited in the procedure. Another option is that the EDX spectra were only collected from the part of the sample that was photographed. Unlike the Pd concentration in the bulk chemical elemental analysis such as the ICP and AAS, therefore it is not representative of the substance. Table 3 shows the results of the data analysis of the main elements in the materials. Beyond those results, the presence of impurities such as Na of 1.041%, S of 2.307%, and K of 3.312% in the GO spectrum indicates that the washing was not optimal,

Table 2. Data analysis of FTIR functional groups of material

Material	O-H	C-H_{sp3}	CO_2	C=O	C=C	C-O
GO	3448.72	2931.80	2337.72	1627.92	1527.62	1095.57, 1249.87
Pd-0.5/RGO	3448.72	2931.80, 2862.36	2337.72	1566.20	1527.62	1203.58
Pd-1.0/RGO	3425.58	2931.80, 2862.36	2337.72	1573.91	1527.62	1149.57, 1211.30
Pd-2.0/RGO	3448.72	2931.80, 2877.79	2337.72	1705.07	1573.91	1219.01

Table 3. Data of the elemental composition of the material from EDX analysis

Material	% Mass C	% Mass O	% Mass Pd	C/O ratio
GO	56.76	38.94	-	1.46
Pd-0.5/RGO	73.43	26.20	0.37	2.80
Pd-1.0/RGO	74.61	24.69	0.70	3.02
Pd-2.0/RGO	75.41	24.11	0.49	3.13

leaving residues of PBS, sulfuric acid, and potassium permanganate.

Analysis of Material Textural Properties

Fig. 4A shows the nitrogen adsorption-desorption isotherm for the produced materials. According to the IUPAC classification, all materials had a type IV isotherm, which corresponded to the features of a mesoporous material. The existence of a hysteresis loop near the isotherm represents this typical mesoporous material. The N_2 sorption isotherm of GO appears to be a sizeable H3-type hysteresis loop with a BET surface area of 69.331 m^2g^{-1} from 0.5 to 1.0 relative pressure. These materials' hysteresis follows the H3 pattern, in which the desorption branch in the closure region tends to be perpendicular to the adsorption branch at lower relative pressures. The material pore pattern of the H3-type loop hysteresis, according to theory, has a wedge or slit geometry resulting from agglomerates of parallel plate-shaped particles [33-34]. The meso- and microporosity of the GO adsorption isotherm can be attributed to the inter-layer gaps between the GO sheets and flaws in the sheets [35]. Metal impregnation, on the other hand, did not affect the overall pore structure. When Pd nanoparticles were deposited on the RGO surface, the type of hysteresis loop changed from H3 to H4, and the specific surface area and pore volume decreased (Table 4). There is a common connection between plate-like particles and the H4 hysteresis loop. The volume of nitrogen adsorption, on the other hand, fell dramatically. This decrease could be due to metal clusters obstructing the holes between the layers [36]. Pd-0.5 and Pd-2.0 have a similar isotherm pattern in that during reduction, they lose substantially all of their microporosity and most of

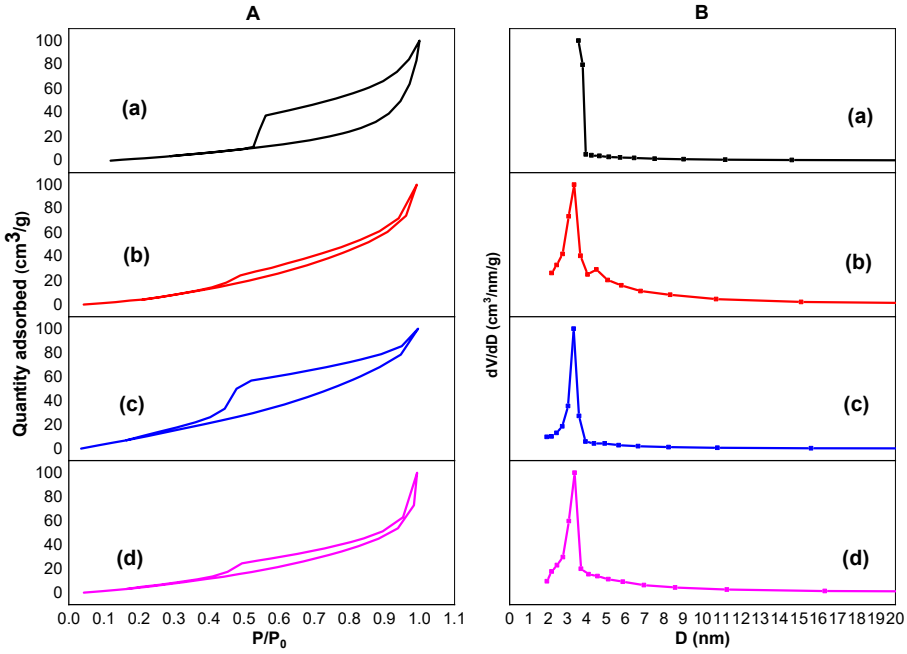

Fig 4. Nitrogen adsorption-desorption isotherm and pore distribution of (a) GO (b) Pd-0.5/RGO (c) Pd-1.0/RGO (d) Pd-2.0/RGO

Table 4. Textural properties of GO and Pd/RGO

Material	Surface area (m^2/g)	Pore volume (cc/g)	Pore diameter (nm)
GO	69.331	0.319	3.566
Pd-0.5/RGO	22.251	0.077	3.350
Pd-1.0/RGO	65.168	0.111	3.316
Pd-2.0/RGO	32.624	0.109	3.372

their mesoporosity, as evidenced by a specific surface area of 20–30 m^2/g [37]. This effect is due to the rearranging and spacing of graphene layers during the reduction process.

Fig. 4B depicts the pore distribution of the materials. The material's pores are mesoporous, ranging from 2 to 50 nm. Based on the BJH desorption method, where all of these materials have a pore diameter of roughly 3 nm, the pore diameter is selected from the highest point on each bar chart, indicating the most frequent pore diameter. Meanwhile, the BET method calculates the specific surface area of materials. Table 4 shows the results of the data analysis of the material's textural qualities. Following a series of treatments, GO transforms into curly RGO, and all Pd/RGO hybrids show a declining trend in BET surface area and pore volume when more metals are added to the hybrid system. Metal nanoparticles inhabited curved graphene surfaces, causing this tendency [38]. According to the investigation results, Pd-1.0/RGO has the most extensive surface area. This large surface area is possible because, when compared to the other two, Pd-1.0 is the most effective loading to be performed on RGO. The metal nanoparticles produced by Pd-1.0 can be distributed evenly. Pd-0.5 is regarded as too small in loading, resulting in infrequent distribution on the RGO surface and no significant increase in the material's specific surface area. Pd-2.0, due to its higher loading weight, is more prone to forming agglomerates between metal nanoparticles when placed on RGO, resulting in a small surface area. Another possibility is that the metals in Pd-0.5/RGO and Pd-2.0/RGO are mostly leached during material washing, resulting in a small surface area. This result is consistent with the percent Pd metal content of Table 3's EDX data.

Analysis of Material Surface Morphology and Nanostructures

Fig. 5 is a collection of SEM pictures. All Pd/RGO materials, including GO, have uneven, rough, wrinkled, and exfoliated sheet-like surfaces. The layered structure of graphene sheets can be seen in the SEM image of GO, according to the literature, with thin layers structured like waves or wrinkles on the surface [39]. The GO sheets had smooth surfaces, similar to what had previously been observed, whereas the RGO sheets had folded folds and wrinkles [40].

The microstructure of GO is depicted in Fig. 6(a), and it is made up of thin, stacked flakes of varied shapes

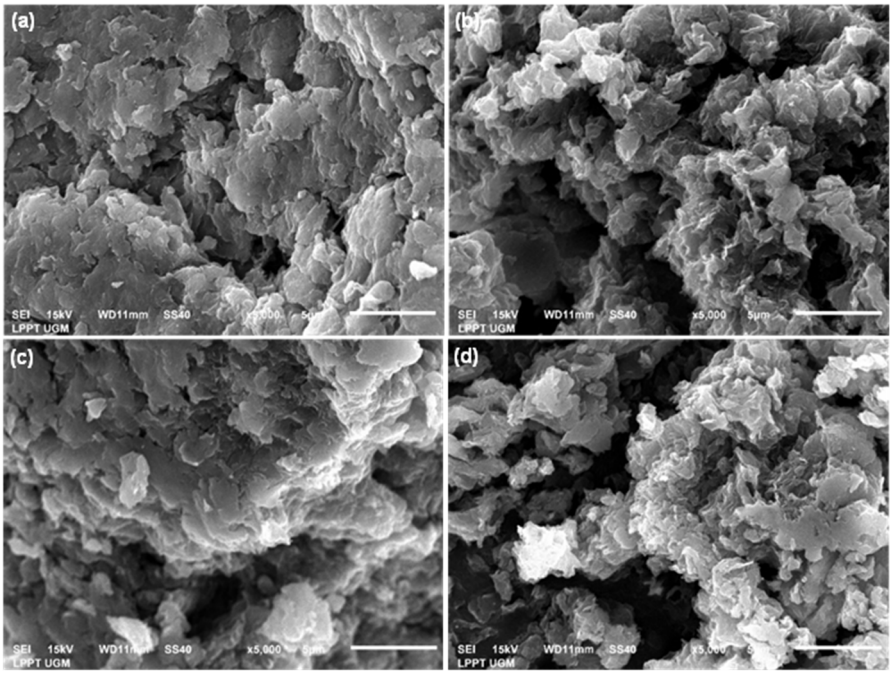

Fig 5. SEM images of (a) GO (b) Pd-0.5/RGO (c) Pd-1.0/RGO (d) Pd-2.0/RGO

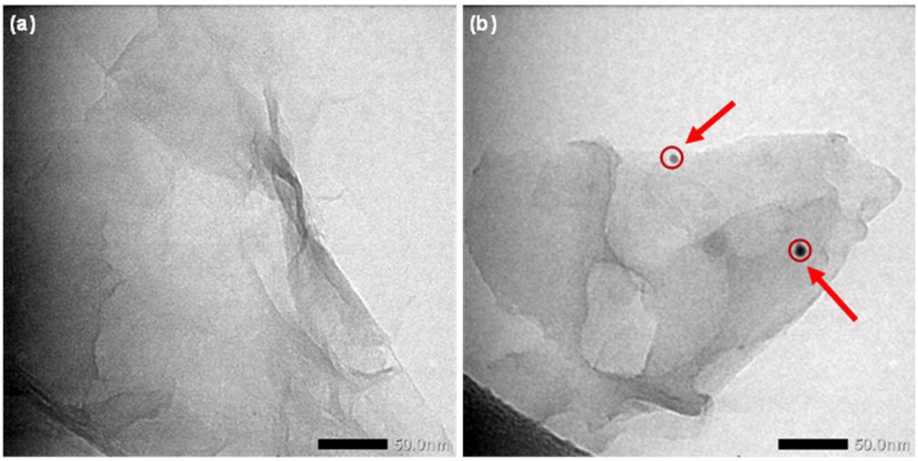

Fig 6. TEM images of (a) GO (b) Pd-2.0/RGO

that have well-defined monolayer and few-layer graphene structures at their edges [41], as well as a smooth platform surface with sporadic folds [42]. The Pd-2.0/RGO micrograph in Fig. 6(b) has a morphology similar to that of GO but with the addition of Pd nanoparticles. The percentage of Pd nanoparticles was found to be low, verified by prior EDX results. Furthermore, the size of the identified Pd-2.0/RGO nanoparticles in Fig. 6(b) is around 10–15 nm, bolstering the XRD findings in Table 1.

■ CONCLUSION

The synthesis of Pd/RGO with microwave assistance has been completed. Although material characterization results did not change significantly, the Pd loading weight on the carrier material did affect particle size, reduction level (C/O), and specific surface area. According to the analysis results, the Pd-1.0/RGO material has the most specific surface area due to the effectiveness of the loading weight towards the distribution of metal nanoparticles produced on the surface of the supporting material. The critical point is that the metal loading should not be too little or too much, as this can result in a small distribution of nanoparticles or even an agglomeration of nanoparticles. Therefore, optimal weight loading of metal on the surface of the supporting material will provide a large material surface area. Several research findings show that increasing the surface area of material improves its performance as a catalyst. Additional research to determine the performance quality of each material is possible through various electrocatalytic applications such as Direct methanol fuel cell (DMFC), Direct formic acid fuel cell (DFAFC), Direct ethanol fuel cell (DEFC), and Oxygen Reduction Reaction (ORR).

■ ACKNOWLEDGMENTS

The authors thank Universitas Gadjah Mada for funding this research through the *Rekognisi Tugas Akhir* (RTA) 2021 scheme with assignment letter number: 3143/UN1.P.III/DIT-LIT/PT/2021 for Triyono.

■ REFERENCES

[1] Dideikin, A.T., and Vul', A.Y., 2019, Graphene oxide and derivatives: The place in graphene family, *Front. Phys.*, 6, 149.

[2] Paulchamy, B., Arthi, G,. and Lignesh, B.D., 2015, A simple approach to stepwise synthesis of graphene oxide nanomaterial, *J. Nanomed. Nanotechnol.*, 6 (1), 253.

[3] Alam, S.N., Sharma, N., and Kumar, L., 2017, Synthesis of graphene oxide (GO) by modified hummers method and its thermal reduction to obtain reduced graphene oxide (rGO), *Graphene*, 6 (1), 1–8.

[4] Kuilla, T., Bhadra, S., Yao, D., Kim, N.H., Bose, S., and Lee, J.H., 2010, Recent advances in graphene based polymer composites, *Prog. Polym. Sci.*, 35 (11), 1350–1375.

[5] Smith, A.T., LaChance, A.M., Zeng, S., Liu, B., and Sun, L., 2019, Synthesis, properties, and applications of graphene oxide/reduced graphene

oxide and their nanocomposites, *Nano Mater. Sci.*, 1 (1), 31–47.

[6] Ranjan, P., Agrawal, S., Sinha, A., Rao, T.R., Balakrishnan, J., and Thakur, A.D., 2018, A low-cost non-explosive synthesis of graphene oxide for scalable applications, *Sci. Rep.*, 8 (1), 12007.

[7] Benzait, Z., Chen, P., and Trabzon, L., 2021, Enhanced synthesis method of graphene oxide, *Nanoscale Adv.*, 3 (1), 223–230.

[8] Marcano, D.C., Kosynkin, D.V., Berlin, J.M., Sinitskii, A., Sun, Z., Slesarev, A., Alemany, L.B., Lu, W., and Tour, J.M., 2010, Improved synthesis of graphene oxide, *ACS Nano*, 4 (8), 4806–4814.

[9] Loryuenyong, V., Totepvimarn, K., Eimburanapravat, P., Boonchompoo, W., and Buasri, A., 2013, Preparation and characterization of reduced graphene oxide sheets via water-based exfoliation and reduction methods, *Adv. Mater. Sci. Eng.*, 2013, 923403.

[10] Abdolhosseinzadeh, S., Asgharzadeh, H., and Kim, H.S., 2015, Fast and fully-scalable synthesis of reduced graphene oxide, *Sci. Rep.*, 5 (1), 10160.

[11] Habte, A.T., and Ayele, D.W., 2019, Synthesis and characterization of reduced graphene oxide (rGO) started from graphene oxide (GO) using the Tour method with different parameters, *Adv. Mater. Sci. Eng.*, 2019, 5058163.

[12] Xie, X., Zhou, Y., and Huang, K., 2019, Advances in microwave-assisted production of reduced graphene oxide, *Front. Chem.*, 7, 355.

[13] Schwenke, A.M., Hoeppener, S., and Schubert, U.S., 2015, Synthesis and modification of carbon nanomaterials utilizing microwave heating, *Adv. Mater.*, 27 (28), 4113–4141.

[14] Mallikarjuna, K., Reddy, L.V., Al-Rasheed, S., Mohammed, A., Gedi, S., and Kim, W.K., 2021, Green synthesis of reduced graphene oxide-supported palladium nanoparticles by *Coleus amboinicus* and its enhanced catalytic efficiency and antibacterial activity, *Crystals*, 11 (2), 134.

[15] Galvan, V., Glass, D.E., Baxter, A.F., and Prakash, G.K.S., 2019, Reduced graphene oxide supported palladium nanoparticles for enhanced electrocatalytic activity toward formate electrooxidation in an alkaline medium, *ACS Appl. Energy Mater.*, 2 (10), 7104–7111.

[16] Çetinkaya, Y., Metin, Ö., and Balci, M., 2016, Reduced graphene oxide supported nickel-palladium alloy nanoparticles as a superior catalyst for the hydrogenation of alkenes and alkynes under ambient conditions, *RSC Adv.*, 6 (34), 28538–28542.

[17] Anasdass, J.R., Kannaiyan, P., Raghavachary, R., Gopinath, S.C.B., and Chen, Y., 2018, Palladium nanoparticle-decorated reduced graphene oxide sheets synthesized using *Ficus carica* fruit extract: A catalyst for Suzuki cross-coupling reactions, *PLoS One*, 13 (2), e0193281.

[18] Wang, B., Yan, T., Chang, T., Wei, J., Zhou, Q., Yang, S., and Fang, T., 2017, Palladium supported on reduced graphene oxide as a high-performance catalyst for the dehydrogenation of dodecahydro-*N*-ethylcarbazole, *Carbon*, 122, 9–18.

[19] Kumar, R., da Silva, E.T.S.G., Singh, R.K., Savu, R., Alaferdov, A.V., Fonseca, L.C., Carossi, L.C., Singh, A., Khandka, S., Kar, K.K., Alves, O.L., Kubota, L.T., and Moshkalev, S.A., 2018, Microwave-assisted synthesis of palladium nanoparticles intercalated nitrogen doped reduced graphene oxide and their electrocatalytic activity for direct-ethanol fuel cells, *J. Colloid Interface Sci.*, 515, 160–171.

[20] Ng, J.C., Tan, C.Y., Ong, B.H., Matsuda, A., Basirun, W.J., Tan, W.K., Singh, R., and Yap, B.K., 2019, Nucleation and growth controlled reduced graphene oxide–supported palladium electrocatalysts for methanol oxidation reaction, *Nanomater. Nanotechnol.*, 9, 1847980419827171.

[21] Li, M., Liu, R., Han, G., Tian, Y., Chang, Y., and Xiao, Y., 2017, Facile synthesis of Pd-Ni nanoparticles on reduced graphene oxide under microwave irradiation for formic acid oxidation, *Chin. J. Chem.*, 35 (9), 1405–1410.

[22] Fatmawati, D.A., Triyono, T., Trisunaryanti, W., and Oktaviano, H.S., and Chasanah, U., 2021, The study of partially and fully oxidized ggraphene oxide prepared by green synthesis for wide-scale fabrication, *Rasayan J. Chem.*, 14, 2129–2135.

[23] Chasanah, U., Trisunaryanti, W., Triyono, T., Oktaviano, H.S., and Fatmawati, D.A., 2021, The performance of green synthesis of graphene oxide prepared by modified hummers method with oxidation time variation, *Rasayan J. Chem.*, 14 (3), 2017–2023.

[24] Fatmawati, D.A., Triyono, T., Trisunaryanti, W., Oktaviano, H.S., and Chasanah, U., 2021, The influence of permanganate enhancement to graphite on chemical structure and properties of graphene oxide material generated by improved Tour method, *Indones. J. Chem.*, 21 (5), 1086–1096.

[25] Shao, G., Lu, Y., Wu, F., Yang, C., Zeng, F., and Wu, Q., 2012, Graphene oxide: The mechanisms of oxidation and exfoliation, *J. Mater. Sci.*, 47 (10), 4400–4409.

[26] Bera, M., Chandravati, C., Gupta, P., and Maji, P.K., 2018, Facile one-pot synthesis of graphene oxide by sonication assisted mechanochemical approach and its surface chemistry, *J. Nanosci. Nanotechnol.*, 18 (2), 902–912.

[27] Prabakaran, K., Jandas, P.J., Mohanty, S., and Nayak, S.K., 2018, Synthesis, characterization of reduced graphene oxide nanosheets and its reinforcement effect on polymer electrolyte for dye sensitized solar cell applications, *Sol. Energy*, 170, 442–453.

[28] Khan, M., Al-Marri, A.H., Khan, M., Mohri, N., Adil, S.F., Al-Warthan, A., Siddiqui, M.R.H., Alkhathlan, H.Z., Berger, R., Tremel, W., and Tahir, M.N., 2014, *Pulicaria glutinosa* plant extract: A green and eco-friendly reducing agent for the preparation of highly reduced graphene oxide, *RSC Adv.*, 4 (46), 24119–24125.

[29] Zhang, J., Feng, A., Bai, J., Tan, Z., Shao, W., Yang, Y., Hong, W., and Xiao, Z., 2017, One-pot synthesis of hierarchical flower-like Pd-Cu alloy support on graphene towards ethanol oxidation, *Nanoscale Res. Lett.*, 12 (1), 521.

[30] Stobinski, L., Lesiak, B., Malolepszy, A., Mazurkiewicz, M., Mierzwa, B., Zemek, J., Jiricek, P., and Bieloshapka, I., 2014, Graphene oxide and reduced graphene oxide studied by the XRD, TEM and electron spectroscopy methods, *J. Electron. Spectrosc. Relat. Phenom.*, 195, 145–154.

[31] Johra, F.T., and Jung, W.G., 2015, Hydrothermally reduced graphene oxide as a supercapacitor, *Appl. Surf. Sci.*, 357, 1911–1914.

[32] Kujur, S., and Pathak, D.D., 2020, Reduced graphene oxide-immobilized iron nanoparticles Fe(o)@rGO as heterogeneous catalyst for one-pot synthesis of series of propargylamines, *Res. Chem. Intermed.*, 46 (1), 369–384.

[33] Thommes, M., Kaneko, K., Neimark, A.V., Olivier, J.P., Rodriguez-Reinoso, F., Rouquerol, J., and Sing, K.S.W., 2015, Physisorption of gases, with special reference to the evaluation of surface area and pore size distribution (IUPAC Technical Report), *Pure Appl. Chem.*, 87 (9), 1051–1069.

[34] Grad, O., Mihet, M., Dan, M., Blanita, G., Radu, T., Berghian-Grosan, C., and Lazar, M.D., 2019, Au/reduced graphene oxide composites: Eco-friendly preparation method and catalytic applications for formic acid dehydrogenation, *J. Mater. Sci.*, 54 (9), 6991–7004.

[35] Shruthi, T.K., Kumar, M.S., Arjunan, M., Pratap, A., and Chandrasekaran, N., 2015, Graphene oxide aided structural tailoring of 3-D *N*-doped amorphous carbon network for enhanced energy storage, *RSC Adv.*, 5 (113), 93423–93432.

[36] Singh, S.B., and De, M., 2021, Improved hydrogen uptake of metal modified reduced and exfoliated graphene oxide, *J. Mater. Res.*, 36 (15), 3109–3120.

[37] Ruiz-Garcia, C., Lei, Y., Heras, F., Elías, A.L., Terrones, M., and Gilarranz, M.A., 2019, Functional Pd/reduced graphene oxide nanocomposites: effect of reduction degree and doping in hydrodechlorination catalytic activity, *J. Nanopart. Res.*, 21 (12), 276.

[38] Wei, L., and Mao, Y., 2016, Enhanced hydrogen storage performance of reduced graphene oxide hybrids with nickel or its metallic mixtures based on spillover mechanism, *Int. J. Hydrogen Energy*, 41 (27), 11692–11699.

[39] Wanderley, K.A., Leite, A.M., Cardoso, G., Medeiros,

A.M., Matos, C.L., Dutra, R.C., and Suarez, P.A.Z., 2019, Graphene oxide and a GO/ZnO nanocomposite as catalysts for epoxy ring-opening of epoxidized soybean fatty acids methyl esters, *Braz. J. Chem. Eng.*, 36 (3), 1165–1173.

[40] Azizighannad, S., and Mitra, S., 2018, Stepwise reduction of graphene oxide (GO) and its effects on chemical and colloidal properties, *Sci. Rep.*, 8 (1), 10083.

[41] Oh, W.C., and Zhang, F.J., 2011, Preparation and characterization of graphene oxide reduced from a mild chemical method, *Asian J. Chem.*, 23 (2), 875–879.

[42] Bugárová, N., Špitálsky, Z., Mičušík, M., Bodík, M., Šiffalovič, P., Koneracká, M., Závišová, V., Kubovčíková, M., Kajanová, I., Zaťovičová, M., Pastoreková, S., Šlouf, M., Majková, E., and Omastová, M., 2019, A multifunctional graphene oxide platform for targeting cancer, *Cancers*, 11 (6), 753.